Cerium-Based Sealing of Anodic Films on AA2024T3: Effect of Pore Morphology on Anticorrosion Performance

A. Carangelo,[a] M. Curioni,[b,*,z] A. Acquesta,[a] T. Monetta,[a] and F. Bellucci[a]

[a]*University of Naples "Federico II", Department of Chemical Engineering, Materials and Industrial Production, 80125 Naples, Italy*
[b]*Corrosion and Protection Centre, School of Materials, The University of Manchester, Manchester M139PL, United Kingdom*

In this work, porous anodic oxides were produced by traditional and modified tartaric sulfuric anodizing (TSA) processes and sealed in hot water, chromate and cerium based solutions. The sealing behavior of a film with relatively coarse porosity, generated at high voltage (traditional TSA), was compared to the sealing behavior of a film with finer porosity and generated at reduced potential (modified TSA). After sodium chromate sealing, the two anodizing cycles produced film with similar anticorrosion performance. Conversely, after hot water or cerium sealing, the finer oxides generated at low voltage (modified TSA) provided much better corrosion resistance. EIS performed in-situ during sealing revealed that chromate sealing is very aggressive to the porous skeleton compared to the other sealing treatments. Therefore, the original morphology has little effect on the final performance, since both fine and coarse oxides are substantially attacked. In contrast, the oxide morphology has a substantial effect when sealing is performed in hot water or cerium-based solution. Overall, it is possible to obtain films with anticorrosion performance equivalent or improved compared to that obtained by traditional TSA anodizing cycle sealed with chromate by combining the low voltage anodizing cycle with the cerium-based sealing.

Manuscript submitted October 4, 2016; revised manuscript received November 7, 2016. Published November 22, 2016.

Aerospace aluminum alloys display outstanding mechanical properties but require specific protection measures in order to meet the requirements of durability and corrosion resistance. Anodizing in acidic electrolytes is one of the methods that are most widely employed for this purpose, since it produces porous oxides that improve corrosion resistance and adhesion with organic coatings.

The porous anodic oxide morphology generated on high copper alloys is significantly different from that generated on high purity aluminium.[1–3] Specifically, on aluminum, anodizing in phosphoric, sulfuric, or oxalic acid, results in the generation of a well-ordered oxide morphology, comprising closely-packed hexagonal cells with a central cylindrical pore, and having a diameter that is proportional to the applied potential.[4–10] Under these conditions, the pore walls are generally straight and uniform (provided that anodizing is conducted under steady applied potential or current). At the bottom of the pores, close to the metal, a barrier layer is observed with thickness proportional to the applied potential. On the other hand, the thickness of the porous oxide is proportional to the charge passed. Due to the dependence of barrier layer thickness and pore diameter on the applied potential, and to the dependence of the film thickness on charge, porous morphologies can be tailored by controlling the electrical regime (potential-time or current-time), and complex morphologies can be achieved to enhance specific properties.[11–14] It has been shown that fine pores and thick films are beneficial for corrosion protection.[13] However fatigue life can be an issue for aerospace alloys[15] and therefore film thickness should be limited to a few microns.

On practical alloys, and on copper containing aerospace alloys in particular, the oxidation behavior of intermetallics and of the copper present in solid solution within the alloy matrix results in a considerably more complex behavior compared to pure aluminium.[2,16–22] In particular, oxidation of copper at the metal-oxide interface results in injection of copper ions into the oxide.[1,18,23–27] The presence of copper ions increases significantly the electronic conductivity within the barrier layer, triggering oxygen evolution within the oxide.[2,18,23,25,28–31] Such oxygen evolution disrupts the well-ordered growth of the aluminum oxide, and induces the formation of a sponge-like morphology.[1,2,18] The geometrical features of such morphology are still dependent on the anodizing potential and charge, i.e. higher anodizing potential produces a coarser morphology, whereas the overall oxide thickness is proportional to the charge passed.[13,14] Thus, the approach of tailoring the oxide morphology by controlled variation of the anodizing potential during the anodizing cycle to enhance the corrosion protection performance can also be applied to practical alloys, and it has been followed previously with success.[12–14,32]

Previous works have shown that in the unsealed condition finer pores, generated at low anodizing potential, provide a much better anticorrosion performance compared to coarser pores, generated at high potential.[12–14,32] However, when anodizing is undertaken at low potential, care must be taken so that the anodizing potential does not fall below the critical value that is necessary for the oxidation of the intermetallics on the alloy surface and for the co-oxidation of alloying elements in solid solution in the matrix. Any residuals of unoxidized noble alloying elements have detrimental effects on the corrosion resistance.[2,17,19,33] The potential required for complete oxidation of second phase particles can be readily identified on some alloys by potentiodynamic anodizing, where peaks in the current versus potential response are associated with the oxidation of specific second phases or, alternatively, from the potential response during galvanostatic anodizing, where potential plateaus are associated with the oxidation of specific intermetallics.[16,17,19,33]

The corrosion protection properties of the anodic oxide can be further enhanced by hydrothermal sealing, a treatment that can be carried out in different electrolytes maintained at elevated temperature.[34–37] Broadly, hydrothermal sealing can be seen as a treatment that involves the partial hydration of the aluminum oxide. Since the hydration products are larger than the original oxide, the porosity can be partially or completely closed by the hydrothermal sealing. Various models have been proposed for hydrothermal sealing of anodized aluminum (i.e. with straight pores), suggesting that initially an outer hydrated layer forms at the pores mouth, separating the electrolyte in the pores from the external electrolyte.[38,39] After the formation of this layer, partial dissolution of the pore wall material occurs, inducing pH increase which ultimately produces the precipitation of hydration products within the pores upon cooling.[40] The composition of the sealing solution, which varies from deionized water to nickel-fluoride or to sodium chromate based electrolytes, affects significantly the processes and the chemical equilibria that regulate the final film properties.[36,41] On copper containing alloys, supporting more complex oxides with globular morphology, most of the works available in the literature

*Electrochemical Society Member.
[z]E-mail: Michele.Curioni@manchester.ac.uk

have focused on the anticorrosion performance rather than the fine details of the sealing mechanism.[35,37,41] Further, on more complex potential-time cycles, typical of industrial practice and resulting in morphologies that vary across the film thickness, the sealing behavior still requires investigation.

This work aims to investigate the effect of pore morphology on the response to sealing treatments, both in terms of sealing behavior and of anticorrosion performance. In particular, the behavior of a typical aerospace anodizing cycle (tartaric – sulfuric acid anodizing identified here as "traditional" TSA[42]) is compared to the behavior of a film obtained in a similar electrolyte (with the exception of an increased concentration of sulfuric acid), but at a lower anodizing potential (identified here as "modified" TSA), such as to generate a much finer pore morphology. Modifications to the TSA cycles, based on lower anodizing potential compared to the traditional TSA, have been previously shown to provide enhanced corrosion protection compared to traditional TSA in the unsealed condition.[12–14,32]

Typically, for aerospace applications, hydrothermal sealing is performed in sodium chromate solutions, but environmental concerns require the development of more environmentally acceptable alternatives. In this work, the effects of the porous oxide morphology on the sealing response and the anticorrosion performance are investigated. Specifically, oxides with two different morphologies (traditional and modified TSA) were sealed in cerium-based solution, sodium chromate solution and hot water. The layers obtained by the cerium-based process were then compared to those obtained by chromate-based sealing, considered as benchmark for anticorrosion performance, and hot water sealing, considered a reference condition where active inhibition is absent. In this context, the advantage of cerium based sealing is to provide a film with high corrosion resistance, without employing toxic chemicals and using a relatively fast process.[43–46] In a previous work, the sealing response of the traditional TSA cycle to the three sealing conditions was investigated in detail and some of the data presented here are taken from there[47] for the purpose of comparison with the response of the modified TSA cycle.

Experimental

Material and pre-treatment.—The material used in this study was AA2024-T3 wrought aluminum alloy. Specimens were obtained from 1.6 mm thick sheets by guillotine, then degreased in acetone, and finally etched in 10 wt% sodium hydroxide at 60°C for 30 s. Final desmutting was carried out in 30 vol. % nitric acid for 15 s at room temperature. Prior to anodizing, the specimens were masked with beeswax, in order to expose an area of 10 cm^2 to the anodizing electrolyte.

Anodizing.—For the traditional TSA cycle, anodizing was undertaken in 0.46 M sulfuric acid with the addition of 0.53 M tartaric acid. Anodizing was performed at 37°C for 20 minutes under potentiostatic control (using a Solartron Modulab potentiostat with high voltage card), following a typical industrial voltage/time cycle (Fig. 1a) involving a voltage ramp and a 20 minutes potentiostatic anodizing at 14 V (SCE). The modified TSA cycle was undertaken in 3.2 M sulphuric acid with the addition of 0.53 M tartaric acid at 25°C. Anodizing was performed under potentiostatic control with a very fast voltage ramp (applied only with the aim of limiting the initial current overshoot) followed by potentiostatic anodizing at 7 V for 20 minutes. The concentration of sulfuric acid for the modified TSA cycle was selected on the basis of previous results,[12–14,32] such as the steady current attained during anodizing at 7 V (25°C) was similar to that attained during anodizing at 14 V and 37°C (circa 8 mA cm^{-2}). As a result, the

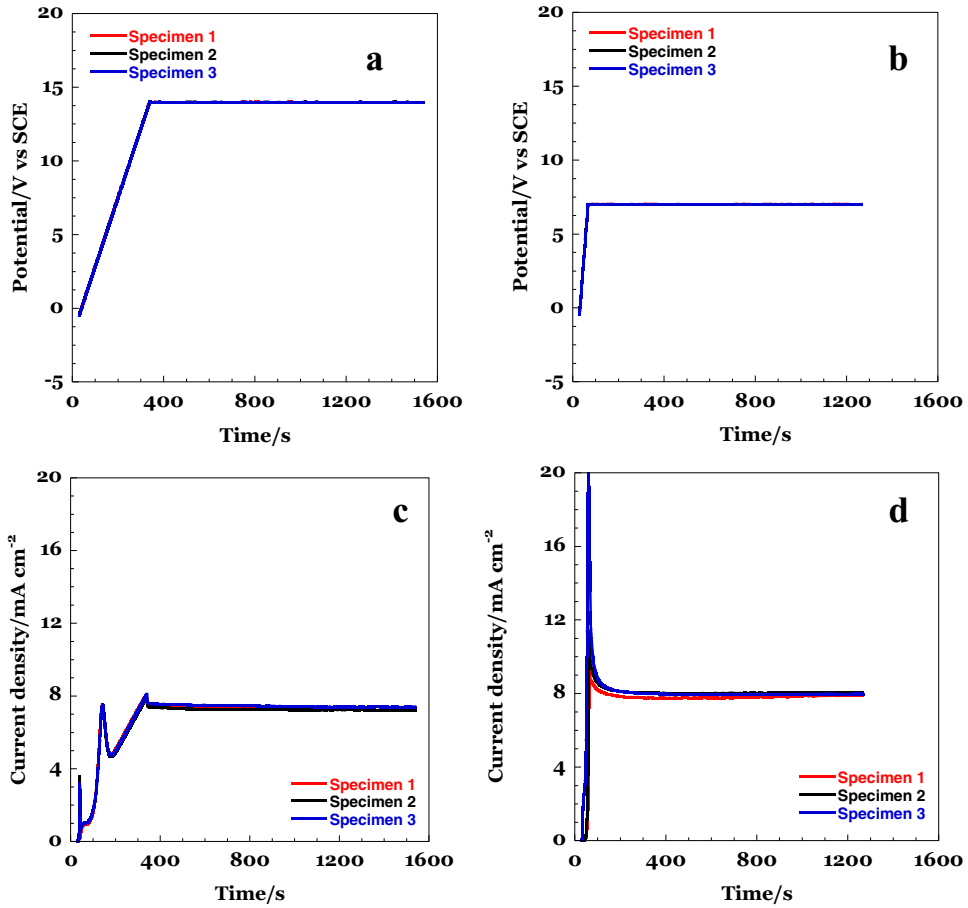

Figure 1. Applied potential-time regimes (a, b) and resulting current responses (c,d) for traditional TSA (a, c) and modified TSA (b, d).

charge passed during both anodizing cycles was closely similar (circa 10.2 C cm^{-2} and 9.5 C cm^{-2} for traditional and modified TSA, respectively), and films with similar thickness could be obtained. Thus, the comparison of the behavior of films with a similar thickness but obtained applying different potential/time regimes enables evaluation of the contributions due to oxide morphology alone. A three-electrode cell was used, with the specimen as the working electrode, a saturated calomel reference electrode and an aluminum cathode. The anodizing electrolyte was stirred during both the anodizing processes. Following anodizing, the specimens were rinsed in deionized water.

Sealing.—After anodizing, three different sealing treatments were applied: cerium-based, chromium based and hot water sealing. During sealing, electrochemical impedance spectra were acquired, as described in detail later. As a control for a condition where no sealing occurs, EIS measurements were also performed on as-anodized specimens immersed in cold water with 1 g/l of sodium sulfate, added to facilitate EIS measurement by increasing the electrolyte conductivity. The solution for cerium (III) nitrate sealing contained 0.015 M hydrated $Ce(NO_3)_3$ and 0.029 M H_2O_2. The role of the hydrogen peroxide was to increase the deposition rate accelerating the oxidation of Ce^{+3} ions to Ce^{+4}. The treatment time was 30 minutes at a temperature of 37°C. Details on the treatment procedure and on the resulting deposits can be found in previous works.[45,47] Chromate sealing was performed in 70 g/l Na_2CrO_4 for 30 minutes at 96°C, whereas hot water sealing was performed in deionized water, with the addition of 1 g/l of sodium sulfate to increase the conductivity, and to enable reliable EIS measurements. The pH was corrected at pH = 6 with sulfuric acid. The treatment required 30 minutes at 96°C.

EIS measurements.—During sealing, EIS was measured with a two-electrode cell, with one specimen as the working electrode (connected to the working and sense cable of the Solartron Modulab potentiostat), and another identical specimen as counter electrode and reference electrode (connected to the counter and reference electrode cables of the potentiostat). The advantages and limitations of this method compared to the traditional three electrodes cell setup, with reference to the systems under investigation here, are discussed in detail elsewhere and not reported here for brevity.[47,48]

During sealing, the EIS spectra were acquired continuously, at 6 minutes intervals. Given that the majority of the time spent to record an EIS spectrum is required to obtain the last few points at low-frequency, the high/medium frequency of the spectrum provides information at 0, 6, 12 minutes and so on, whereas the low frequency points are acquired in the later stage of each individual time interval. The issues related to acquisition of EIS spectra during sealing of porous anodic oxides are discussed elsewhere[47] and the discussion is not reported here for brevity. The frequency range inspected varied from 100 kHz to 20 mHz, and the applied potential perturbation was 10 mV.

Following sealing, EIS was also carried out in 1 M Na_2SO_4 solution at room temperature, to characterize the films after all the dissolution and precipitation processes had terminated. In this case, a three-electrode cell was used and the low-frequency limit for the acquisition of the spectra was extended to 5 mHz. Before EIS, the open circuit potential was monitored for 15 minutes. Each electrochemical test was repeated three times in order to evaluate the reproducibility; generally, very minor differences (of the order of 10% of the impedance modulus), if any, between repeated tests were found. EIS spectra in 3.5 wt% sodium chloride solutions were measured at regular intervals with the same three electrodes setup and amplitude. The frequency range inspected varied from 100 kHz to 5 mHz. Between measurements, the specimens were left to corrode freely in the sodium chloride solution.

Results

Anodizing.—Anodizing was carried out according to two different electrical regimes, as depicted in Figure 1. The first electrical regime (traditional TSA) is the typical cycle applied in industry for the tartaric-sulfuric anodizing process and involves an initial potential ramp from 0 to 14 V (SCE) during the first 5 minutes of anodizing, followed by 20 minutes of potentiostatic anodizing at 14 V (SCE). The time evolution of the applied potential is presented in Figure 1a. The alternative electrical regime (modified TSA), involved a much faster potential ramp (0.2 V/s) followed by a potentiostatic hold at 7 V (SCE) and was performed in the electrolyte with higher concentration of sulfuric acid maintained at room temperature. The initial fast potential ramp in this cycle is not required to improve the properties of the anodic oxide, but it has been applied here to avoid current overloading in the potentiostat, which has a limit of 100 mA and interrupts the experiment in case of overloading. With a conventional two electrode power supply that is capable of self-limiting current in case of overload without interrupting the test, the first ramp would not be required.

The current responses presented in Figures 1c, 1d indicate that the steady current during the potentiostatic hold in the two conditions was very similar (in the region of 8 mA cm^{-2}). This is due to the fact that the lower anodizing potential is applied in the more concentrated solution. This result is expected, since these conditions have been selected based on previous works focusing on optimization of the anodizing cycles.[12–14,32] The aim here was to generate films with comparable thickness but different oxide morphologies. In particular, traditional TSA exhibits very fine pores in the outer regions, generated initially at low potential during the ramp, which progressively coarsen toward the metal interface. The majority of the film, thus, has a coarse morphology, generated during high potential step at 14 V. In contrast, oxides generated with the modified TSA have much finer pores throughout the thickness and do not display the outer regions of very fine porosity, since the initial ramp is fast and terminates before the pores fully nucleate. All the morphological aspects associated with the two processes are presented and discussed in detail elsewhere.[12–14,32] It is worth also noticing that the oxides obtained by traditional and modified TSA are expected to have a very similar chemical composition, since the only difference between the two anodizing electrolytes is the concentration of sulfuric acid.

Concerning the electrical response recorded during the initial ramp, for the traditional TSA process, two peaks, associated with the oxidation of second phases were clearly visible. During the fast ramp applied in the second cycle, peaks in the current response were not clearly visible, since the charge passed was not sufficient to induce complete oxidation of the second phases, but only to generate a thin oxide layer on the alloy surface. After the ramp was terminated, the current decreased rapidly, to attain a steady value after approximately 200 seconds. Such decrease is associated with the initial thickening of the oxide layer, followed by pore nucleation and propagation.[2,11] Simultaneously, second phase oxidation occurs.

Sealing.—Figure 2 presents the impedance spectra recorded on the two porous anodic oxides immediately and after 24 minutes of immersion in cold water with the addition of sodium sulfate. This is considered the control condition, where no sealing occurs in both cases. Clearly, the impedance spectra are dominated by the capacitive response associated with the presence of the barrier layer beneath the pores. Interestingly, in the control condition, the values of low-frequency impedance associated with the modified TSA cycle were slightly higher than that of the traditional TSA cycle.

The impedance response measured during sealing in hot water for both anodizing cycles is reported in Figure 3. For clarity, only the first spectrum (acquired immediately after immersion) and the last spectrum (acquired between 24 and 30 minutes of immersion approximatively) are reported here. No major differences are observed for both treatments compared to the cold water control condition, except a slight increase in the low frequency values of the modulus of impedance with increasing sealing time. The behavior during sealing in sodium chromate (Figure 4) was markedly different. In particular, a significant increase in capacitance (evident as a left shift of the medium-frequency regions of the spectra) was observed during the sealing process, and an increase in the low-frequency values of the

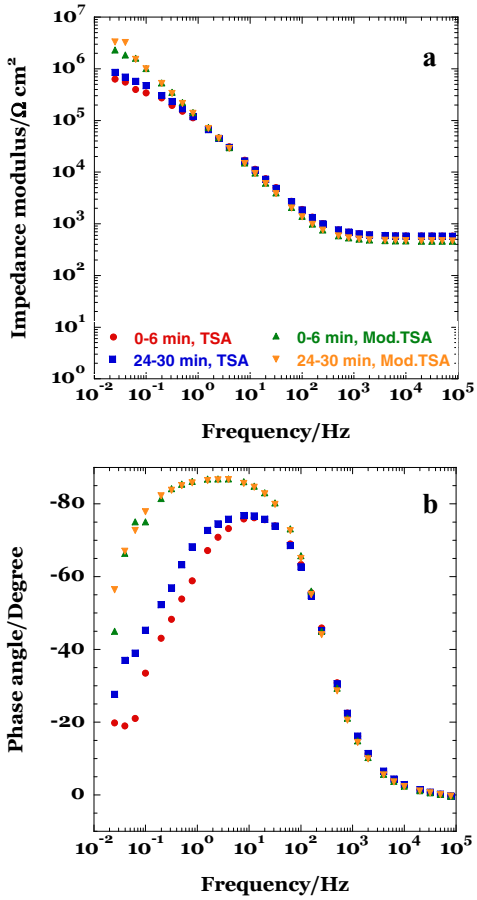

Figure 2. EIS spectra acquired from specimens supporting porous anodic oxides generated by traditional TSA and by modified TSA. Spectra presented were acquired immediately after and after 24 minutes of immersion in the cold water solution.

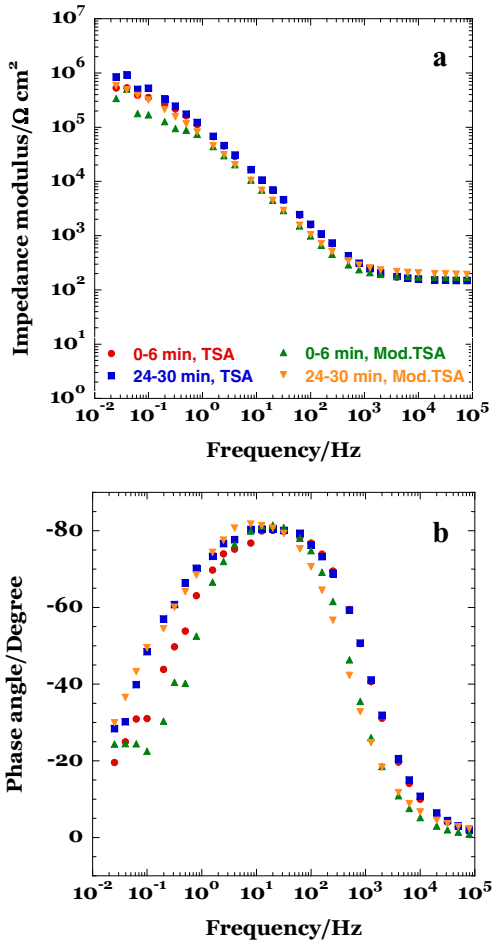

Figure 3. EIS spectra acquired from specimens supporting porous anodic oxides generated by traditional TSA and by modified TSA. Spectra presented were acquired immediately after and after 24 minutes of immersion in the hot water solution.

impedance modulus. However, the increase in capacitance was proportionally more significant for the films obtained in the traditional TSA compared to those obtained with the modified TSA process. From previous study, such increase in capacitance observed during chromate sealing is due to a substantial thinning of the barrier layer due to the relatively aggressive sealing solution. The impedance spectra obtained during cerium sealing are presented in Figure 5. For both anodic oxides, no variation in capacitance during sealing was observed, indicating little or no attack of the barrier layer. However, for the traditional TSA cycle, a slight increase in low frequency values of the impedance modulus was revealed. On the other hand, the modified TSA cycle showed virtually no variation during the sealing process, but the initial value was significantly higher than for traditional TSA.

Figure 6 presents the comparison of the impedance spectra measured in the cold solution of sodium sulfate after the various sealing treatments were applied. It is evident that the qualitative effect of each treatment was similar for both the anodizing cycles. Furthermore, the second time constant that appeared in the medium frequency range in hot water and cerium treatments, was more evident for the specimens anodized by the modified TSA process. This second time constant is evident only after sealing, when the measurement is performed at low temperature, because it is associated to the precipitation of the hydrated sealing products within the pores. During sealing, at higher temperature, such hydrated products are in the form of gels and, due to the relatively low resistance, cannot be resolved by EIS measurement.[47]

EIS measurements during corrosion.—After the selected anodizing and sealing treatments, the specimens were immersed in 3.5 wt% NaCl and impedance measurements were taken at regular intervals for 14 days. In Figure 7, the results obtained from the control unsealed specimens are presented. During the 336 hours of immersion, for both anodizing treatments, a progressive decrease in values of impedance was observed. However, such decrease was more marked for the specimen anodized with the traditional TSA cycle, which attained a low frequency value of impedance modulus of 10^4 ohm cm^2 after 336 hours. The low-frequency impedance modulus of the specimen anodized by the modified TSA cycle also decreased with time, but the final value was approximately one order of magnitude higher. Importantly, a substantial increase in capacitance, evident as a shift toward the left of the EIS spectra, was revealed for the traditional TSA process, whereas such increase was almost absent for the modified TSA process. Further, the modified TSA process displayed a new high-frequency time constant for long immersion times, which was not evident for the traditional TSA process.

The behavior measured after hot water sealing (Fig. 8) was significantly different. Both anodizing treatments maintained high values of impedance throughout the test duration. Some decrease in the low-frequency values was observed for the specimens anodized in the traditional TSA. Both treatments displayed a reduction of the contribution of the medium-frequency time constant with increasing immersion times, but such reduction was more marked for the specimens anodized by the modified TSA cycle. During corrosion of the specimen anodized by the traditional TSA cycle and sealed in sodium chromate (Fig. 9), a decrease in low-frequency impedance values was observed after 7 days, and a significant increase in capacitance was evident

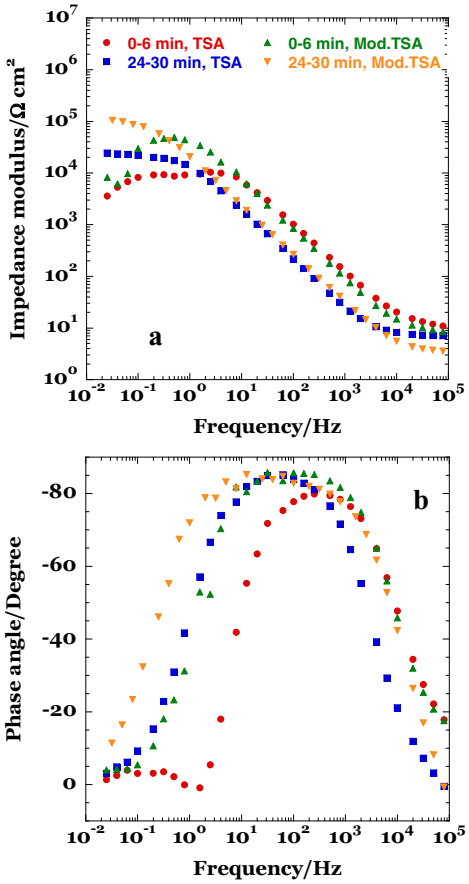

Figure 4. EIS spectra acquired from specimens supporting porous anodic oxides generated by traditional TSA and by modified TSA. Spectra presented were acquired immediately after and after 24 minutes of immersion in the sodium chromate solution.

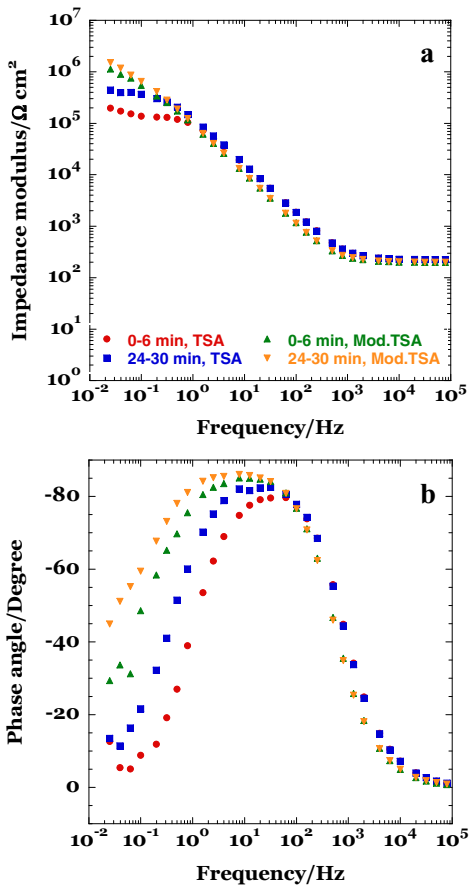

Figure 5. EIS spectra acquired from specimens supporting porous anodic oxides generated by traditional TSA and by modified TSA. Spectra presented were acquired immediately after and after 24 minutes of immersion in the cerium-based solution.

between 168 and 336 hours. Such behavior was much less evident on the specimens anodized with the modified TSA cycle. In particular, the decrease in impedance modulus was moderate and no increase in capacitance was observed during the 336 hours immersion time. The specimens anodized by traditional TSA and subsequently cerium-sealed (Fig. 10) displayed a progressive decrease in impedance values over 336 hours, with a corresponding increase in capacitance. This was not observed for the specimens anodized by the modified TSA cycle, which did not show an increase in capacitance or a substantial drop in the low-frequency impedance values. Both cycles exhibited an additional high frequency time constant, which was more visible, and increased more, with increasing immersion time.

Corrosion imaging.—In order to corroborate the EIS results, couples of anodized and sealed specimens were masked and immersed vertically in 3.5 wt% NaCl solution, at the free corrosion potential. In Figures 11–14, the surface appearance of the specimens during corrosion is compared. It is evident that the sealing treatment that provided the best anticorrosion performance was the cerium-based treatment, followed by the chromate treatment and the hot-water sealing. Further, the modified TSA cycle was substantially better than the traditional TSA cycle, with no sign of corrosion after cerium treatment and minimal corrosion after hot water and after chromate sealing. Similar trends were observed for the worst of the two specimens, i.e. the cerium treatment was the more protective, and the modified TSA produced the best anticorrosion performance. Overall, cerium treatment on modified TSA provided better anticorrosion performance when compared to the sodium chromate sealing of traditional TSA.

Discussion.—The interaction between porous oxide morphology, sealing behavior and corrosion resistance on practical aluminum alloys is complex, since many parameters contribute to the overall behavior. In this work, in order to understand such interaction and produce sealed oxide with anticorrosion performance similar or higher than the industrial benchmark (traditional TSA sealed with chromates), two anodic oxide films, with similar thickness but different morphology, were produced. The modification in morphology was attained by modifying the electrical regime, since the applied potential directly correlates with the pore diameter on pure aluminum and with the characteristic dimensions of the globular morphology on aluminium-copper alloys. In particular, it is well known that the traditional TSA oxide displays a porosity that is relatively closed in the external regions, since these are generated during the early stages of the potential ramp, thus at low potential, and relatively coarse throughout the majority of the thickness, since it is generated later during the stage of high potential hold. Conversely, the modified TSA cycle displays a much finer porosity throughout the thickness, since the film is generated by anodizing at 7 V.

The EIS spectra acquired in the cold control conditions (not aggressive to the oxide or to the alloy, Figure 2) already reveal significant differences between the oxides generated by the two treatments. In particular, it is evident that the oxide generated at lower potential has a slightly higher capacitance (consistent with a thinner barrier layer) but higher low-frequency impedance modulus. This observation suggests that the low-frequency impedance modulus is not uniquely determined by the thickness of the barrier layer on the multiphase alloy under study, since if this was the case a thinner barrier layer would necessarily also be associated to a lower impedance modulus. In

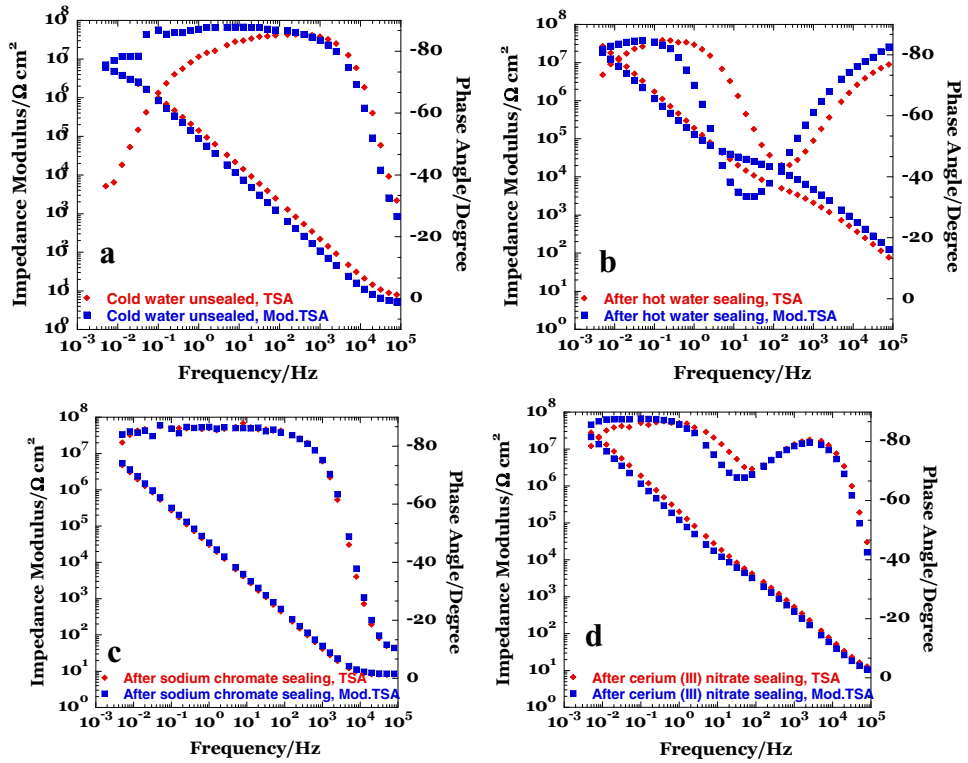

Figure 6. EIS spectra acquired at room temperature in 1M Na_2SO_4, a) unsealed oxides, b) hot water sealed oxides, c) sodium chromate sealed oxides and d) cerium sealed oxides. Comparison between responses of the oxides generated by traditional TSA (red diamonds) and modified TSA (blue squares).

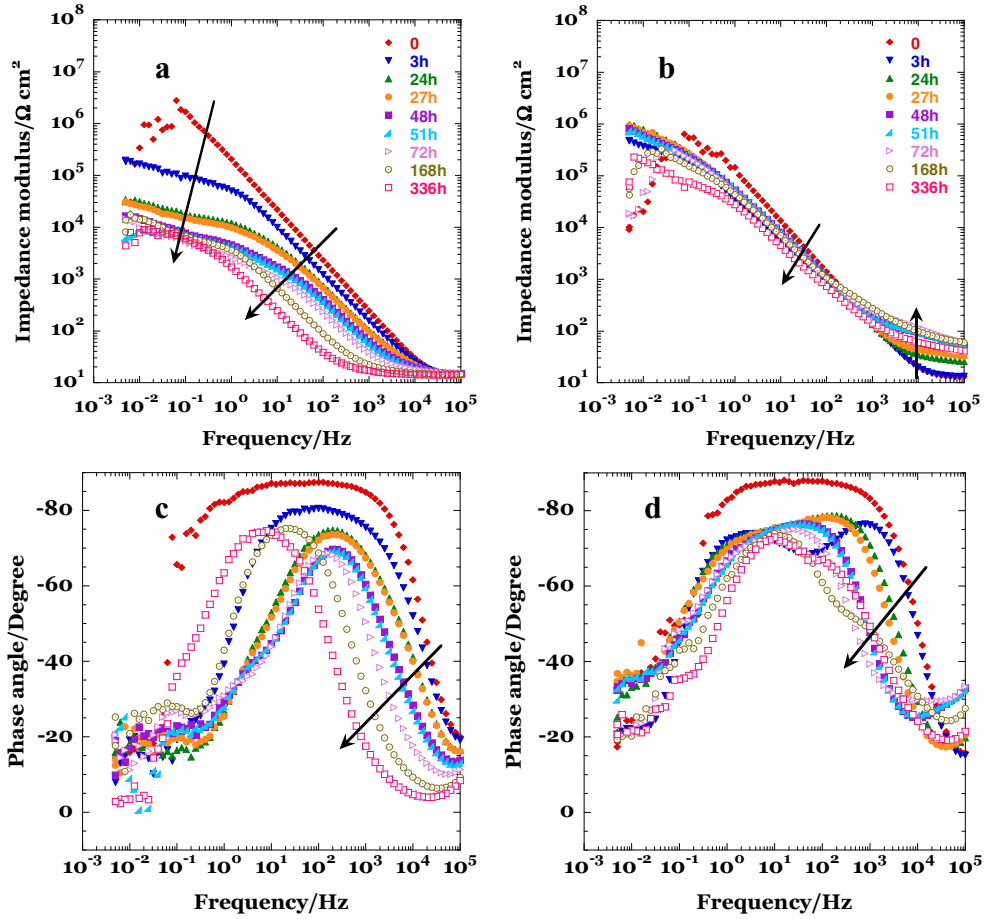

Figure 7. Series of EIS spectra of unsealed anodic oxides obtained during 336 hours of exposure in 3.5% NaCl: a, c) TSA and b, d) modified TSA.

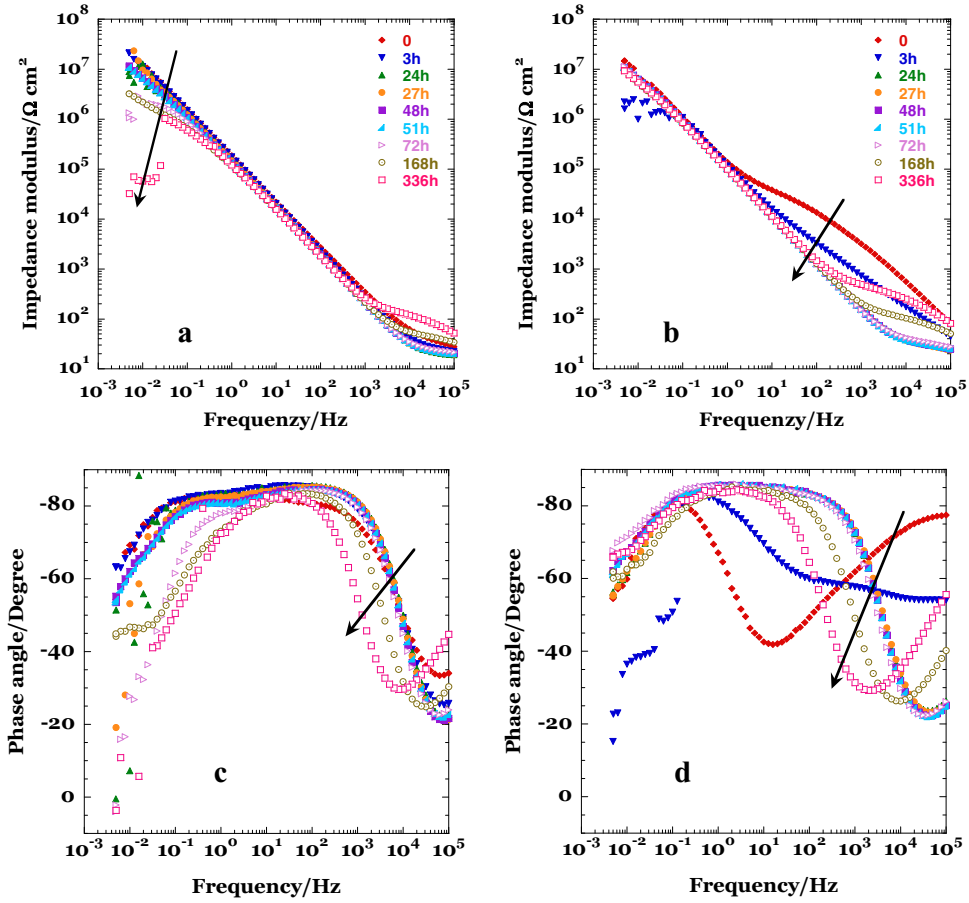

Figure 8. Series of EIS spectra of hot water sealed anodic oxides obtained during 336 hours of exposure in 3.5% NaCl: a, c) TSA and b, d) modified TSA.

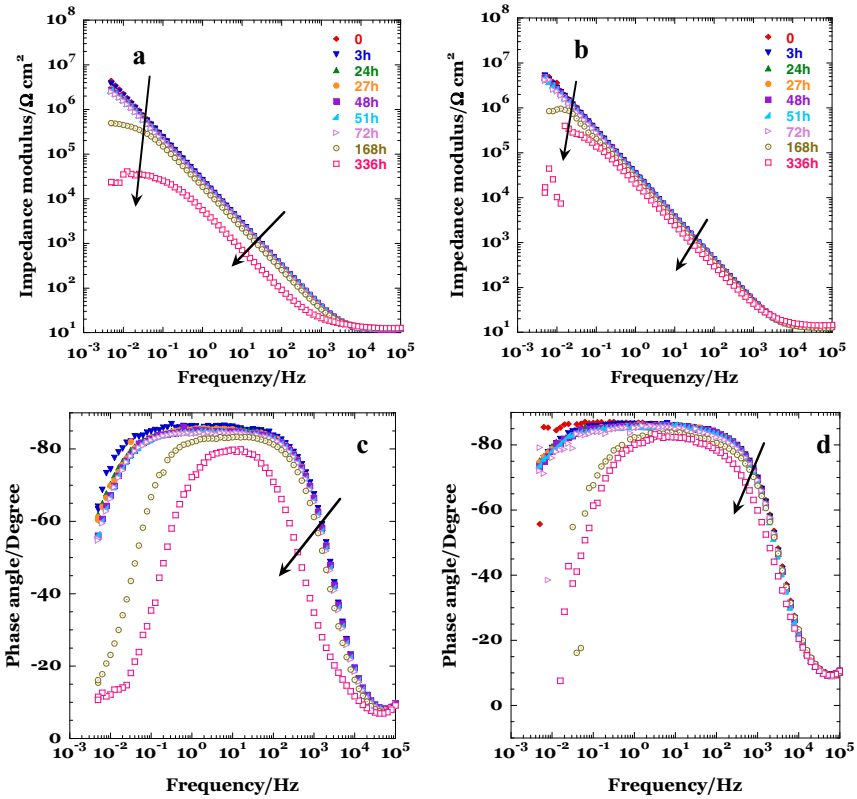

Figure 9. Series of EIS spectra of chromate sealed anodic oxides obtained during 336 hours of exposure in 3.5% NaCl: a, c) TSA and b, d) modified TSA.

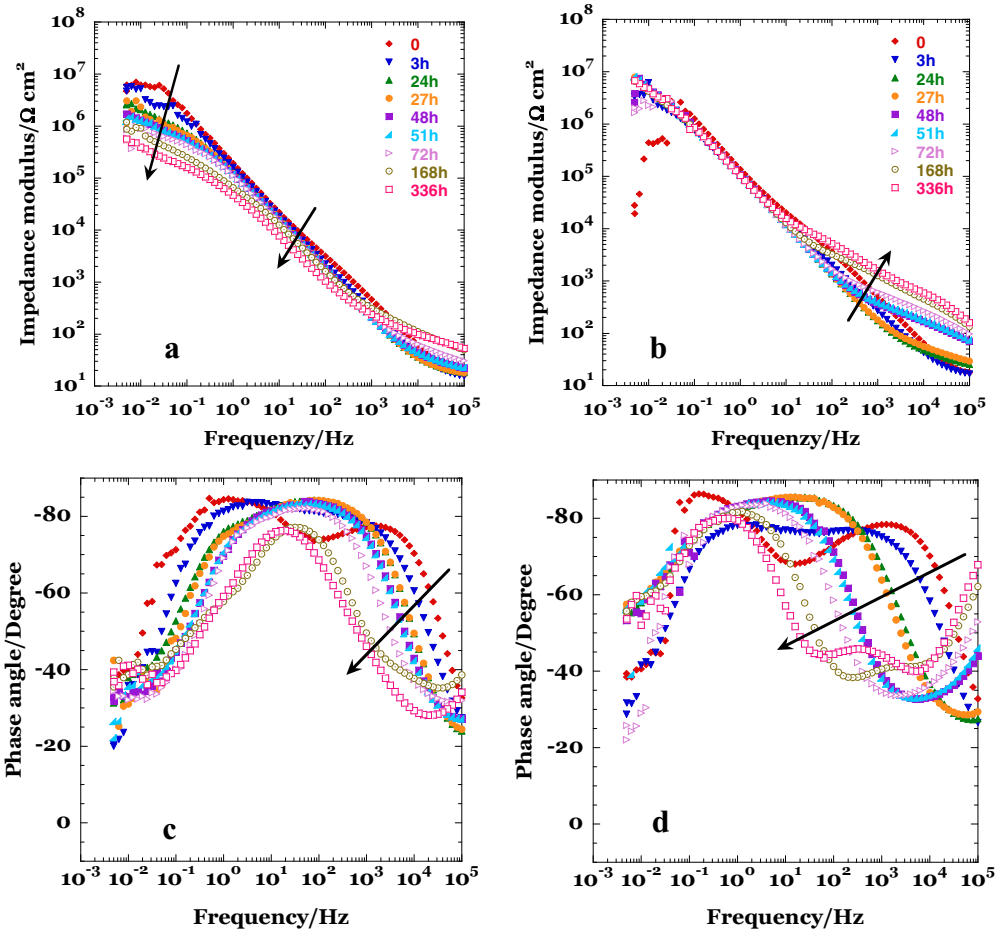

Figure 10. Series of EIS spectra of cerium sealed anodic oxides obtained during 336 hours of exposure in 3.5% NaCl: a, c) TSA and b, d) modified TSA.

reality, after anodizing, a number of surface defects at various scales might be present on the alloy surface, such as partially oxidized second phases or regions with defective oxide. Thus, the overall EIS response is given not only by the properties of the film on the alloy matrix (dominated by the barrier layer thickness) but also by the properties of the morphologically and chemically different oxide formed on the second phase material, intrinsically more defective than the oxide formed on the matrix, due to the abundant oxygen evolution associated to the oxidation of copper during anodizing. Considering that the low-frequency limit of the impedance is significantly higher

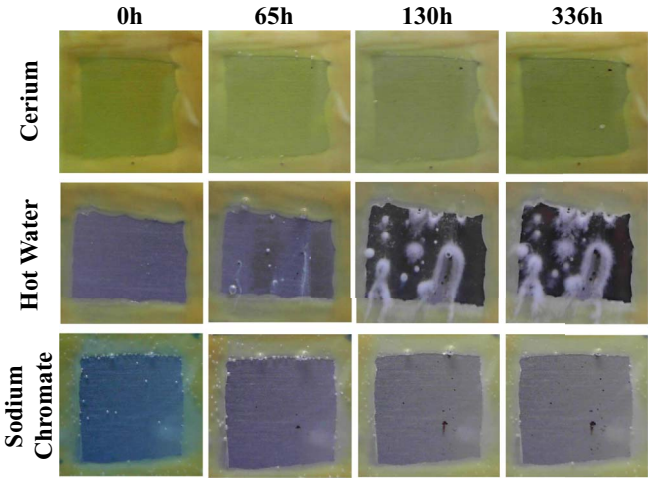

Figure 11. Surface appearance during corrosion in 3.5 wt% NaCl of the specimens anodized by the traditional TSA process and sealed with the different treatments. Pairs of nominally identical specimens were corroded and this figure reports the specimen appearing less corroded.

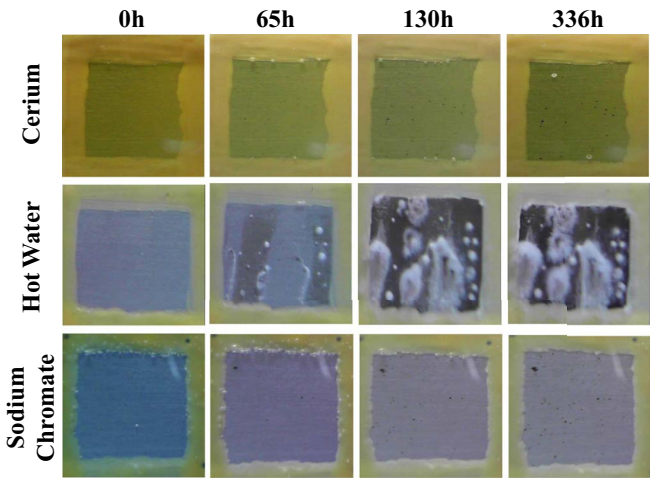

Figure 12. Surface appearance during corrosion in 3.5 wt% NaCl of the specimens anodized by the traditional TSA process and sealed with the different treatments. Pairs of nominally identical specimens were corroded and this figure reports the specimen appearing more corroded.

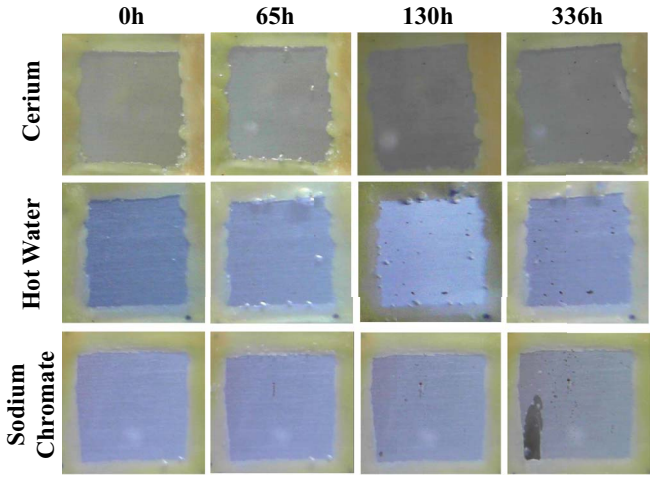

Figure 13. Surface appearance during corrosion in 3.5 wt% NaCl of the specimens anodized by the modified TSA process and sealed with the different treatments. Pairs of nominally identical specimens were corroded and this figure reports the specimen appearing less corroded.

for the modified TSA cycle compared to the traditional TSA, it is reasonable to conclude that the lower anodizing potential is beneficial in reducing the number and the area of such defective oxide regions.

The behavior during the various sealing treatments (Figs. 3–5) also indicates that the anodic oxides obtained with the modified TSA process respond better to sealing. In particular, higher values of low-frequency impedance modulus are consistently observed during the last cycle of the in situ EIS measurements. This can be rationalized again by considering the reduced presence of defects in the oxides generated by the modified TSA process. The differences in EIS response associated with the various sealing treatments on a specific porous anodic oxide have been discussed in detail previously,[47] and are not discussed further here. Upon cooling, the precipitation of the sealing products takes place, followed by crystallization. After sealing, the comparison between the two treatments is of particular interest; clearly, the time constant present at medium frequency range and associated with the precipitation of the sealing products was more pronounced for the modified TSA process compared to the traditional TSA. This can be rationalized by considering that finer pores are much easier to completely seal once the precipitation processes are triggered.

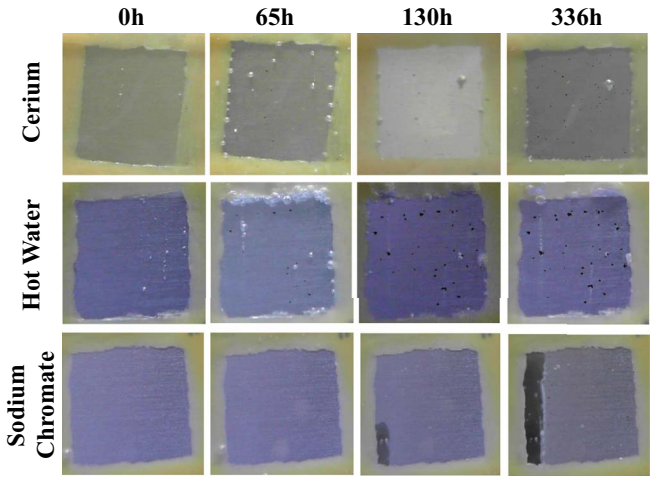

Figure 14. Surface appearance during corrosion in 3.5 wt% NaCl of the specimens anodized by the modified TSA process and sealed with the different treatments. Pairs of nominally identical specimens were corroded and this figure reports the specimen appearing more corroded.

The analysis reported above directly provides the basis for interpreting the observed corrosion behaviors. The modified TSA process, due to the finer porosity that is more impervious to the penetration of aggressive species (in the unsealed condition) and that respond better to sealing, consistently displayed an impedance that is much higher than the traditional TSA process, as evident from the EIS spectra acquired during corrosion in 3.5 wt% NaCl. The behavior revealed by EIS was mirrored by the observations from real time imaging of the corroding surfaces. On traditional TSA, the anticorrosion performance of cerium sealing was comparable with that of chromate sealing, with only minor signs of corrosion after 328 hours. On the modified TSA process, with reduced pore diameter, the corrosion performance of both hot water and cerium sealing was significantly increased compared to that of films generated in traditional TSA and subsequently sealed in the same solutions. In contrast, the performance of chromate sealing was similar or marginally worse. These observations can be rationalized considering that chromate sealing is much more aggressive to the pre-existing anodic oxides (as revealed by in-situ EIS measurement here and discussed in detail previously[47]) and the anticorrosion performance arises from active inhibition provided by the residual chromate ions, rather than from an improvement in barrier effect. Thus, given the aggressiveness of chromium sealing and the active inhibition due to chromate ions, the geometry of the initial porous skeleton is not particularly important in determining the anticorrosion performance after sealing. In contrast, for the other two treatments (hot water and cerium based), the geometry of the pre-existing anodic oxide is much more important, since it is not disrupted as much as for chromate sealing. For hot water sealing, the improvement in corrosion resistance is mainly due to barrier effects associated with the precipitation of hydrated products and pore closure. Thus, if the pore geometry is finer, it is easier to be filled homogeneously by hydration products. Similar arguments apply to the cerium sealing, where the hydration of the porous skeleton is less important, but a significant precipitation of cerium products occurs within and above the pores, as shown by the appearance of the second time constant (see Fig. 6).

Overall, the experimental evidence presented here indicates that the combined use of the modified TSA anodizing cycle, together with cerium based sealing, produces film with anticorrosion performance that is equivalent or exceeds that of chromate sealed traditional TSA. This is due to the effect of the fine pore morphology that enhances the barrier properties and facilitates the sealing, combined with the active inhibition provided by cerium ions.

Conclusions

In this work, the effect of the anodizing treatment on the sealing response and corrosion behavior after sealing was investigated for AA2024T3. Two treatments were compared: traditional TSA, producing a film with relatively coarse morphology, and modified TSA, producing a film with much finer porosity. The specimens anodized with the two treatments were sealed by three different processes: sodium chromate, hot water, and cerium based sealing. EIS performed during sealing indicated that the finer morphology obtained by the modified TSA cycle responded better during sealing, as evident by higher values of low frequency impedance. Post sealing measurements performed in non-aggressive electrolytes also indicated that the porosity was more closed for the specimens obtained by modified TSA, for all of the sealing treatments. In agreement, the anticorrosion performance of the modified TSA process was consistently better than that of the traditional TSA, regardless of the sealing method. Finally, the combination of modified TSA anodizing cycle with cerium sealing produced oxides with properties comparable, if not superior, to those that are achieved by chromate sealed traditional TSA.

Acknowledgments

The authors thank EPSRC for the support of the LATEST2 Programme grant (EP/H020047/1) and of the STEPFAR Programme grant (PON 03PE_00129_1).

References

1. L. Iglesias-Rubianes, S. J. Garcia-Vergara, P. Skeldon, G. E. Thompson, J. Ferguson, and M. Beneke, *Electrochimica Acta*, **52**, 7148 (2007).
2. M. Curioni, M. Saenz De Miera, P. Skeldon, G. E. Thompson, and J. Ferguson, *Journal of the Electrochemical Society*, **155**, C387 (2008).
3. K. Shimizu, K. Kobayashi, G. E. Thompson, and P. Skeldon, *Corrosion Science.*, **39**(2), 281 (1997).
4. J. P. O'Sullivan and G. C. Wood, *Proceedings of the Royal Society of London. Series A, Mathematical and Physical Sciences*, **317**, 511 (1970).
5. R. C. Furneaux, G. E. Thompson, and G. C. Wood, *Corrosion Science*, **18**, 853 (1978).
6. G. E. Thompson, R. C. Furneaux, J. S. Goode, and G. C. Wood, *Transactions of the Institute of Metal Finishing*, **56**, 159 (1978).
7. S. J. Garcia-Vergara, P. Skeldon, G. E. Thompson, and H. Habakaki, *Applied Surface Science*, **254**, 1534 (2007).
8. S. J. Garcia-Vergara, P. Skeldon, G. E. Thompson, and H. Habakaki, *Corrosion Science*, **49**, 3696 (2007).
9. P. Skeldon, G. E. Thompson, S. J. Garcia-Vergara, L. Iglesias-Rubianes, and C. E. Blanco-Pinzon, *Electrochemical and Solid-State Letters*, **9**, B47 (2006).
10. F. Zhou, A. K. Mohamed Al-Zenati, A. Baron-WiecheÄ‡, M. Curioni, S. J. Garcia-Vergara, H. Habazaki, P. Skeldon, and G. E. Thompson, *Journal of the Electrochemical Society*, **158**, C202.
11. M. Curioni, P. Skeldon, and G. E. Thompson, *Journal of the Electrochemical Society*, **156**, C407 (2009).
12. M. Curioni, P. Skeldon, J. Ferguson, and G. E. Thompson, *Journal of Applied Electrochemistry*, **41**, 773 (2011).
13. M. Curioni, P. Skeldon, G. E. Thompson, and J. Ferguson, in *Advanced Materials Research*, 48 (2008).
14. M. Curioni, P. Skeldon, G. E. Thompson, and J. Ferguson, *ECS Transactions*, 41 (2008).
15. A. Scala, A. Squillace, T. Monetta, D. B. Mitton, D. Larson, and F. Bellucci, *Surface and Interface Analysis*, **42**, 194 (2010).
16. Y. Ma, X. Zhou, G. E. Thompson, M. Curioni, T. Hashimoto, P. Skeldon, P. Thomson, and M. Fowles, *Journal of the Electrochemical Society*, **158**, C17 (2011).
17. M. Saenz de Miera, M. Curioni, P. Skeldon, and G. E. Thompson, *Corrosion Science*, **52**, 2489 (2010).
18. M. Curioni, F. Roeth, S. J. Garcia-Vergara, T. Hashimoto, P. Skeldon, G. E. Thompsona, and J. Ferguson, *Surface and Interface Analysis*, **42**, 234 (2010).
19. M. Saenz De Miera, M. Curioni, P. Skeldon, and G. E. Thompson, *Surface and Interface Analysis*, **42**, 241 (2010).
20. L. Domingues, J. C. S. Fernandes, M. Da Cunha Belo, M. G. S. Ferreira, and L. Guerra-Rosa, *Corrosion Science*, **45**, 149 (2002).
21. J. Cote, E. E. Howlett, and H. J. Lamb, *Plating*, **57**, 484 (1970).
22. A. K. Mukhopadhyay and A. K. Sharma, *Surface and Coatings Technology*, **92**, 212 (1997).
23. X. Zhou, G. E. Thompson, P. Skeldon, G. C. Wood, K. Shimizu, and H. Habazaki, *Corrosion Science*, **41**, 1089 (1999).
24. M. Abulsain, A. Berkani, F. A. Bonilla, Y. Liu, M. A. Arenas, P. Skeldon, G. E. Thompson, P. Bailey, T. C. Q. Noakes, K. Shimizu, and H. Habazaki, *Electrochimica Acta*, **49**, 899 (2004).
25. M. A. Paez, T. M. Foong, C. T. Ni, G. E. Thompson, K. Shimizu, H. Habazaki, P. Skeldon, and G. C. Wood, *Corrosion Science (USA)*, **38**, 59 (1996).
26. H. Habazaki, X. Zhou, K. Shimizu, P. Skeldon, G. E. Thompson, and G. C. Wood, *Electrochimica Acta*, **42**, 2627 (1997).
27. S. Garcia-Vergara, P. Skeldon, G. E. Thompson, P. Bailey, T. C. Q. Noakes, H. Habazaki, and K. Shimizu, *Applied Surface Science*, **205**, 121 (2003).
28. Y. Liu, E. A. Sultan, E. V. Koroleva, P. Skeldon, G. E. Thompson, X. Zhou, K. Shimizu, and H. Habazaki, *Corrosion Science*, **45**, 789 (2003).
29. H. Habazaki, K. Shimizu, M. A. Paez, P. Skeldon, G. E. Thompson, G. C. Wood, and X. Xhou, *Surface and Interface Analysis*, **23**, 892 (1995).
30. S. J. Garcia-Vergara, K. El Khazmi, P. Skeldon, and G. E. Thompson, *Corrosion Science*, **48**, 2937 (2006).
31. T. Dimogerontakis, L. Kompotiatis, and I. Kaplanoglou, *Corrosion Science (USA).*, **40**(11), 1939 (1998).
32. M. Curioni, A. A. Zuleta, E. Correa, X. Pan, A. Baron-Wiechec, P. Skeldon, J. G. Castaño, F. Echeverría, and G. E. Thompson, *Transactions of the Institute of Metal Finishing*, **90**, 290 (2012).
33. M. Saenz de Miera, M. Curioni, P. Skeldon, and G. E. Thompson, *Corrosion Science*, **50**, 3410 (2008).
34. Y. Xingwen, C. Chunan, and Y. Zhiming, *Journal of Materials Science Letters*, **19**, 1907 (2000).
35. F. Mansfeld, C. Chen, C. B. Breslin, and D. Dull, *Journal of the Electrochemical Society*, **145**, 2792 (1998).
36. Y. Shang, L. Wang, Z. Liu, D. Niu, Y. Wang, and C. Liu, *International Journal of Electrochemical Science*, **11**, 5234 (2016).
37. G. Boisier, N. Pebere, C. Druez, M. Villatte, and S. Suel, *Journal of the Electrochemical Society*, **155** (2008).
38. M. R. Kalantary, D. R. Gabe, and D. H. Ross, *Journal of Applied Electrochemistry*, **22**, 268 (1992).
39. V. Lopez, E. Otero, A. Bautista, and J. A. Gonzalez, *Surface and Coatings Technology*, **124**, 76 (2000).
40. V. López, M. J. Bartolom, E. Escudero, E. Otero, and J. A. González, *Journal of the Electrochemical Society*, **153** (2006).
41. Y. Zuo, P. H. Zhao, and J. M. Mao, *Surface and Coatings Technology*, **166**, 237 (2003).
42. E. P. EP1233084.
43. S. You, P. Jones, A. Padwal, P. Yu, M. O'Keefe, W. Fahrenholtz, and T. O'Keefe, *Materials Letters*, **61**, 3778 (2007).
44. S. Joshi, E. A. Kulp, W. G. Fahrenholtz, and M. J. O'Keefe, *Corrosion Science*, **60**, 290 (2012).
45. I. V. Gordovskaya, T. Hashimoto, J. Walton, M. Curioni, G. E. Thompson, and P. Skeldon, *Journal of the Electrochemical Society*, **161**, C601 (2014).
46. T. Monetta, A. Acquesta, V. Maresca, R. Signore, F. Bellucci, P. D. Petta, and M. L. Masti, *Surface and Interface Analysis*, **45**, 1522 (2013).
47. A. Carangelo, M. Curioni, A. Acquesta, T. Monetta, and F. Bellucci, *Journal of the Electrochemical Society*, **163**, C619 (2016).
48. M. Curioni, F. Scenini, T. Monetta, and F. Bellucci, *Electrochimica Acta*, **166**, 372 (2015).